Energetics of discrete selectivity bands and mutation-induced transitions in the calcium-sodium ion channels family

I. Kaufman[1], D. G. Luchinsky[1,2], R. Tindjong[1],
P.V.E. McClintock[1], R.S. Eisenberg[3]
[1]*Department of Physics, Lancaster University, Lancaster LA1 4YB, UK**
[2]*NASA Ames Research Center, MS 269-3, Moffett Field, CA, 94035, USA and*
[3]*Department of Molecular Biophysics and Physiology,*
Rush Medical College, 1750 West Harrison, Chicago, IL 60612, USA
(Dated: May 9, 2013)

We use Brownian dynamics simulations to study the permeation properties of a generic electrostatic model of a biological ion channel as a function of the fixed charge Q_f at its selectivity filter. We are thus able to reconcile the recently-discovered discrete calcium conduction bands M0 ($Q_f = 1e$), M1 ($3e$), M2 ($5e$) with the set of sodium conduction bands L0 (0.5-0.7e), L1 (1.5-2e) thereby obtaining a completed pattern of conduction and selectivity bands *vs.* Q_f for the sodium-calcium channels family. An increase of Q_f leads to an increase of calcium selectivity: L0 (sodium selective, non-blocking channel) → M0 (non-selective channel) → L1 (sodium selective channel with divalent block) → M1 (calcium selective channel exhibiting the anomalous mole fraction effect). We create a consistent identification scheme where the L1 band is identified with the eukaryotic (DEKA) sodium channel, and L0 (speculatively) with the bacterial NaChBac channel. The scheme created is able to account for the experimentally observed mutation-induced transformations between non-selective channels, sodium-selective channels, and calcium-selective channels, which we interpret as transitions between different rows of the identification table. By considering the potential energy changes during permeation, we show explicitly that the multi-ion conduction bands of calcium and sodium channels arise as the result of resonant barrier-less conduction. Our results confirm the crucial influence of electrostatic interactions on conduction and on the Ca^{2+}/Na^{+} valence selectivity of calcium and sodium ion channels. The model and results could be also applicable to biomimetic nanopores with charged walls.

PACS numbers: 87.16.Vy, 41.20.Cv, 05.40.-a, 87.10.Mn

I. INTRODUCTION

At the molecular level, an understanding of living systems requires the application of physics and this is particularly true in the case of biological ion channels. Here, we study the physics of a simple electrostatic model to investigate the operation of voltage-gated calcium and sodium ion channels. Their importance arises because they play an essential role in controlling muscle contraction, in neurotransmitter secretion, gene regulation and the transmission of action potentials. The effective function of calcium channels is based on their high selectivity for divalent calcium ions Ca^{2+} over monovalent sodium ions Na^{+}. They exhibit the anomalous mole fraction effect (AMFE), an effective blockade of Na^{+} permeation by small concentrations of Ca^{2+}, combined with measurable Ca^{2+} currents in the pA range [1, 2]. Sodium channels have very similar structure but demonstrate the opposite kind of selectivity, favouring Na^{+} over Ca^{2+}.

The selectivity of calcium and sodium channels is defined by a narrow selectivity filter with a strong binding site formed by protein residues with a net negative charge Q_f whose magnitude depends on the particular protein residues [60] that are present. The L-type calcium channel has a highly-conserved EEEE locus with four glutamates [3], whereas the RyR channel has a DDDD locus [4]. The DDDD locus was also found in the TRPV6 transient receptor potential channel, which is highly calcium-selective but generally very different from the RyR channel [5].

Sodium channels have structures very similar to those of calcium channels, but with different selectivity filter loci (and therefore different Q_f), and different lengths and radii [6–8]. The eukaryotic sodium channel has a DEKA locus with a inferred $Q_f \approx 1e$ [6, 8] where $e = -1.6 \times 10^{-19}$ C is the electronic charge. Bacterial sodium channels can have rather different selectivity filter loci: from LEAWAS in NaChBac channel [9] to L-type-like EEEE in the recently-studied bacterial NavAb channel [7, 10].

Experimental studies of mutations in the protein side chains [9, 11–15], and model simulations [8, 16, 17], show that the value of Q_f is a crucial factor in determining the Ca^{2+} *vs.* Na^{+} selectivity of calcium and sodium channels. Usually, mutations that influence Q_f also destroy the calcium channel's selectivity, and hence physiological functionality, leading to "channelopathies" [13, 18]. However, an appropriate point mutation of the DEKA sodium channel ($Q_f \approx 1e$) converts it into a calcium-selective channel with a DEEA locus and $Q_f \approx 4e$ [11]. The essentially non-selective bacterial OmpF porin ($Q_f \approx 1e$) can be converted into a Ca^{2+}-selective channel by the in-

*Electronic address: p.v.e.mcclintock@lancaster.ac.uk

troduction of two additional glutamates in the constriction zone; the resultant mutant contains a DEEE-locus ($Q_f \approx 4e$) and exhibits an Na^+ current with a strongly increased sensitivity to 1 mM Ca^{2+} [15].

The mechanisms of Ca^{2+}/Na^+ selectivity underlying these transformations have remained unclear, as has also the complete and unambiguous identification of the "charge – selectivity type" relationship.

Multi-ion knock-on barrier-less conductivity [61] is assumed to be one of the main mechanisms of permeation and selectivity for the potassium [19, 20] and calcium [21, 22] channels, and inferred to be a general mechanism of selectivity [23]. Barrier-less knock-on conductivity can also be described as a limiting case of long-range ion-ion correlations [24, 25].

Generic electrostatic models describe an ion channel as a cylindrical water-filled hole in a charged protein in the cell membrane. They usually assume single-file motion of the permeating ions and can reproduce significant features related to the conductivity and selectivity [26–31]. Thus a single model with almost unchanging parameters can account for the valence selectivity features of both sodium and calcium channels (reviewed in [32, 33]).

We have recently used parametric Brownian dynamics (BD) simulations of ionic currents for different Q_f in a generic model of calcium channels to show that the Ca^{2+} conduction and Ca^{2+}/Na^+ valence selectivity form a regular pattern of narrow conduction/selectivity bands as a function of Q_f, separated by regions of non-conduction (one of the conduction bands was simulated earlier in [34]). These discrete bands relate to saturated, self-sustained Ca^{2+} conductivity with different numbers of ions involved in the conduction. We have associated the underlying mechanism with multi-ion barrier-less conductivity, identified the calcium selective bands seen in the simulations with known calcium channels, and inferred that the band structure could explain the results of mutant studies [35, 36]. The idea that channel conduction might be a discontinuous function of channel parameters with pass bands and stop bands was discussed at length in the speculations of one of us, long ago [37].

In this paper we complete the ordered sequence of Ca^{2+} and Na^+ conduction and Ca^{2+}/Na^+ selectivity bands *vs.* surface charge Q_f for the sodium-calcium channels family initiated in [35]. We add an analysis of sodium bands and construct an identification table to explain and classify numerous mutation-induced transformations of Ca^{2+}/Na^+ selectivity in the calcium-sodium channels family. We also investigate the energetics of the generic electrostatic model and consider potential energy profiles along optimal multi-ion stochastic trajectories [30, 38] to show that the calcium and sodium conduction and selectivity bands are based on the barrier-less conduction mechanism.

We start by summarising in Sec. II the main features of the generic model. In Sec. III A we describe the ordered sequence of selectivity types for sodium-calcium channels family based on BD simuations of the model [35]. We relate these data to real ion channels in Sec. III B and to mutation-induced transformation between them in III C. In Secs. III D and III E we work out the energetics of permeation and show how the observed bands correspond to optimal conditions (minimal energy barrier) for one-ion and two-ion processes respectively. Finally, in Sec. IV we summarise and draw conclusions.

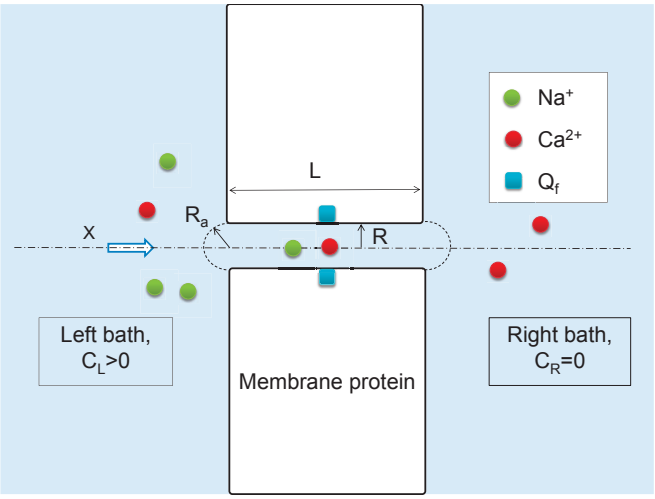

FIG. 1: (Color online) Computational domain for a generic model of the calcium ion channel. Its selectivity filter is treated as an axisymmetric, water-filled, cylindrical hole of radius $R = 3$ Å and length $L = 12 - 16$ Å through the protein hub in the cellular membrane. There is a centrally-placed, uniformly-charged, rigid ring of negative charge $Q_f = 0{-}6.5e$. The left-hand bath, modeling the extracellular space, contains non-zero concentrations of Ca^{2+} or Na^+ ions. These are injected at the Smoluchowski diffusion rate at radius R_a. The domain length L_d=100 Å, the domain radius R_d = 100Å, the grid size $h = 0.5$ Å, and a potential difference of 0–75 mV is applied between the left and right domain boundaries.

II. A GENERIC ELECTROSTATIC MODEL OF CALCIUM CHANNELS

The self-consistent electrostatic model of calcium/sodium channel that we will use represents the channel's selectivity filter as a negatively-charged, axisymmetric, water-filled protein hub in the cell membrane as shown in Fig. 1. It is a generic model of a calcium ion channel similar to that used previously [26, 34, 39]. The negatively-charged ionized protein residues are modeled as a single, thin, uniformly-charged, centrally-placed, rigid ring around the selectivity filter bringing a net negative charge within the range $0 < Q_f < 6.5e$. The extracellular (left) and intracellular (right) baths are taken to be filled with ionic sodium-only, calcium-only, or mixed sodium-calcium aqueous solutions. In what follows we assume an asymmetrical ionic concentration: $C_L > 0$ on the left, and $C_R = 0$ on the right corresponding to physiological conditions in

calcium and sodium channels. Details of the model have already been presented and its validity and limitations discussed [35], but for completeness we now summarise it briefly.

The minimum possible radius R of the selectivity filter of an L-type calcium channel has been determined as being $R = 2.8\,\text{Å}$. We use the value of $R = 3.0\,\text{Å}$. The mobile sodium and calcium ions are described as charged spheres of radius $R_i \approx 1\,\text{Å}$ (matching both ions), with diffusion coefficients of $D_{Na} = 1.17 \times 10^{-9}$ m^2/s and $D_{Ca} = 0.79 \times 10^{-9}$ m^2/s, respectively. The domain length $L_d = 100\,\text{Å}$, the domain radius $L_r = 100\,\text{Å}$, and the grid size is $h = 0.5\,\text{Å}$. A voltage in the range $V = 0 - 75\,\text{mV}$ was applied between the left and right domain boundaries.

We take both the water and the protein to be homogeneous continua with dielectric constants $\varepsilon_w = 80$ and $\varepsilon_p = 2$, respectively, together with an implicit model of ion hydration (the validity of which is discussed elsewhere). We approximate ε_w and D as equal to their bulk values throughout the whole computational domain, including the selectivity filter, a choice that avoids the use of arbitrary fitting parameters.

The importance of self-consistent calculations cannot be overstated. If calculations are not self-consistent, then the potential does not take proper account of all the charges that are present. Thus, some of the potential has a mysterious nonphysical origin. In the real world,and in experiments, conditions and concentrations change. Consistent calculations determine the potential that results from these changes [33].

The electrostatic field was derived by self-consistent numerical solution of Poisson's equation:

$$-\nabla(\varepsilon\nabla u) = \frac{\sum_i e z_i n_i}{\varepsilon_0} \tag{1}$$

where ε_0 is the dielectric permittivity of vacuum, ε is the dielectric permittivity of the medium (water or protein), u is the electric potential, e is the elementary charge, z_i is the charge number (valence), and n_i is the number density of ions. We used a finite volume Poisson solver with a staggered grid particularly designed to account for large permittivity gradients.

The huge gradient between $\varepsilon_w = 80$ and $\varepsilon_p = 2$ results in quasi-1D axial behavior of the electrostatic field, and hence in axial movement of positive ions inside the channel. Single-file behavior is thus the result of the forces in the model, as is the binding and selectivity in closely related models [39–41]. The combined influences of the dielectric boundary force and the interaction with the fixed charge prohibit the entrance of any negatively charged ions [42]. Consequently, we can use a 1D dynamical model to approximate the axial, single-file, movement of cations (only) inside the selectivity filter and in its close vicinity.

The BD simulations were based on numerical solution of the 1D over-damped time-discretized Langevin equation for i-th ion:

$$\frac{dx}{dt} = -Dz(\frac{\partial u}{\partial x}) + \sqrt{2D}\xi(t) \tag{2}$$

where x stands for the ion's position, D is its diffusion coefficient, z is the valence, u is the self-consistent potential at the location x in (k_BT/e) units, K_B is Bolzmann constant, T is tempetature and $\xi(t)$ is normalized white noise. Numerical solution of (2) was implemented with the Euler forward scheme.

We use an ion injection scheme that allows us to avoid wasteful and heavy-duty simulation of ionic movements in the bulk liquid. The model includes a hemisphere of radius $R_a = R$ at each entrance representing the boundaries between the channel vicinity and the baths. The arrival rate j_{arr} is connected to the bulk concentration C through the Smoluchowski diffusion rate: $j_{arr} = 2\pi D R_a C$ [27, 43, 44].

This reduced model obviously represents a considerable simplification of the actual electrostatics and dynamics of moving ions and water molecules within the narrow selectivity filter [45, 46]. Nonetheless, simulations based on this model [17, 34, 35] reproduce reasonably well the signatures of calcium channels, such as their AMFE [2]. Despite their oversimplifications, models of this sort account quantitatively for the detailed properties of the RyR channel and have allowed predictions of complex current–voltage relations before the corresponding experiments had been done, with errors of less than 10% [4].

The model is generic in the sense that it is just based on electrostatics and on the fundamental physical properties of channels with simplified geometric shape. It takes no account of the detailed structure of the proteins or residues and treats water and protein as continuum dielectrics with their respective dielectric constants. Hence it could equally well be applied to biomimetic nanotubes [47, 48], or to TPRV channels [5], that have similar geometry and surface charge.

III. RESULTS AND DISCUSSION

A. The pattern of calcium and sodium conduction and selectivity bands

Fig. 2 presents results from Brownian dynamics simulations of permeation for the generic channel model. Fig. 2(a) shows the pronounced regular structure in the Ca^{2+} ion current J_{Ca} as a function of Q_f. It consists of narrow regions of high conductance (conduction bands) M0, M1, M2 separated by almost zero-conductance stop-bands. The peak separation $\Delta Q \approx 2e$ corresponds to the charge on one Ca^{2+} ion. Peaks of J correspond to transition regions in P, where P jumps from one saturated integer value to the next one, while zero-conductance bands correspond to regions of constant P. This kinetics phenomenon will be discussed later. These bands are

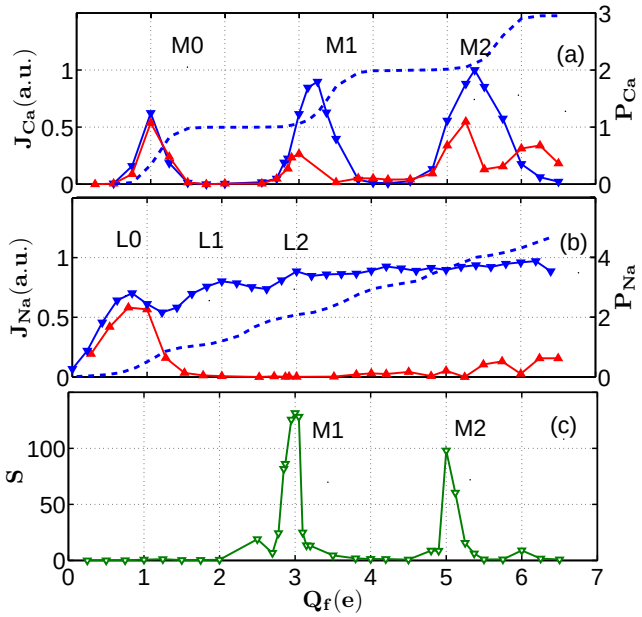

FIG. 2: (Color online) Multi-ion conduction, selectivity and occupancy bands of the generic ion channel model (partly reworked from [35]). (a) Plots of the calcium current J_{Ca} as a function of the fixed charge Q_f at the selectivity filter for pure (blue, point-down, triangles) and mixed (red, point-up, triangles) baths show distinct, clearly-resolved, conduction bands M0, M1, and M2. Peaks in conduction for the pure bath correspond to transitions of occupancy P_{Ca} (blue, dashed). (b) Plots of the sodium current J_{Na} as a function of Q_f for pure (blue, point-down, triangles) and mixed (red, point-up, triangles) baths show weakly resolved overlapped conduction bands L0, L1, L2. Smoothened peaks in conduction in pure bath corresponds to smoothened transitions of occupancy P_{Na} (blue, dashed). (c) A plot of the selectivity ratio $S = J_{Ca}/J_{Na}$ for the mixed salt shows selectivity growth from L0 to M0, following by plateau near L1 and strong peaks corresponding to the M1 and M2 calcium bands.

presented both for a bath of pure $CaCl_2$ and for a mixed salt configuration. The bands M1 and M2 are significantly attenuated in the mixed salt as compared to the pure one. Band M1 coincides with the J *vs.* Q_f peak simulated earlier for an L-type channel [34].

In Fig. 2(b) the sodium current is plotted *vs.* Q_f for a pure NaCl bath and for a mixed salt configuration. For the pure bath, J_{Na} *vs.* Q_f exhibits weak local maxima that we can treat as analogous to the calcium conduction bands in (a). We label them as L0, L1, L2, corresponding to integer sodium occupancy $P_{Na} = 1, 2, 3$ of the selectivity filter; these broad bands overlap and never fall to zero, making the sodium conductance relatively independent of Q_f. The separations of the L-band maxima are half the size of those in the calcium M-bands, reflecting the charge difference between Na^+ and Ca^{2+} ions. The sodium current in the mixed salt bath exhibits a persistent block for $Q_f >$ M0.

The appearance of the distinct conduction bands is caused by ion-ion and ion-fixed charge electrostatic interaction and by the discreteness of the multi-ion occupancy P [23, 30]. Their strong contrast for Ca^{2+} in the calcium channel relates to the double-valence of Ca^{2+}, enhancing the electrostatic effects of valence selectivity [28]. It will be shown explicitly below (see Secs. III D and III E) that both the calcium and sodium conduction bands correspond to resonance-like barrier-less conductivity.

Fig. 2(c) plots the selectivity ratio $S = J_{Ca}/J_{Na}$ showing how the channel is selective in favor of calcium in a mixed salt bath. The sequence starts from $S \approx 0.01$ for L0 (sodium-selective channel), increases for $S \approx 1$ (non-selective channel) for M0, slightly drops near L1 (sodium-selective channel) and starts to increase sharply after L1 reaches a high peak of selectivity $S \approx 130$ for the calcium selective peak M1, corresponding to the L-type calcium channel. Note that calcium selectivity peaks M1 and M2 are shifted to lower Q_f related to correspondent peaks of J (see (a)) and correspond to the threshold of P transitions. We will discuss these phenomena below.

B. Identification of selectivity bands in the calcium/sodium channels family

We now try to relate the observed charge-ordered sequence of conduction and selectivity bands shown in Fig. 2 to the behaviour exhibited by real channels in experiments. Calcium and sodium conduction and stop bands divide the Q_f axis into a number of distinct regions differentiated by the type of Ca^{2+}/ Na^+ selectivity, i.e. by combination of 4 features: the Na^+ conductivity for a pure bath; the Ca^{2+} conductivity for a pure bath; the existence and power of the divalent block; and the AMFE (i.e. selective calcium current), for the mixed salt bath. Combining these features we can find several clearly differentiated Q_f regions with distinct selectivity types related to particular channels including wild-type, mutants, and artificial.

Fig. 3 shows that the band L0 ($Q_f \approx 0.6e$) demonstrates moderate sodium conductivity and small calcium conductivity for both the pure and mixed baths (plot (a)), and there is no divalent block or AMFE (plots (a), (b)). Calcium ions just cannot overcome the self-potential barrier and enter the channel leading to near-zero P_{Ca} (plots (b), (c)) for all values of $[Ca]$. As a result L0 represents a non-blocking sodium-selective channel. We may speculate that this band is associated with the bacterial sodium NaChBac channel [9], which exhibits a similar type of selectivity; such a connection was also proposed recently by Corry [49].

Fig. 4 shows that the M0 channel ($Q_f \approx 1e$) exhibits non-selective conduction and occupancy for both sodium and calcium (plots (a), (b)), and non-selective time-sharing mutual occupany profiles (plot (c)) and thus represents a non-selective cation channel. It may be identified with the non-selective cation channel described in [50] or the OmpF channel [15]. The high calcium J cor-

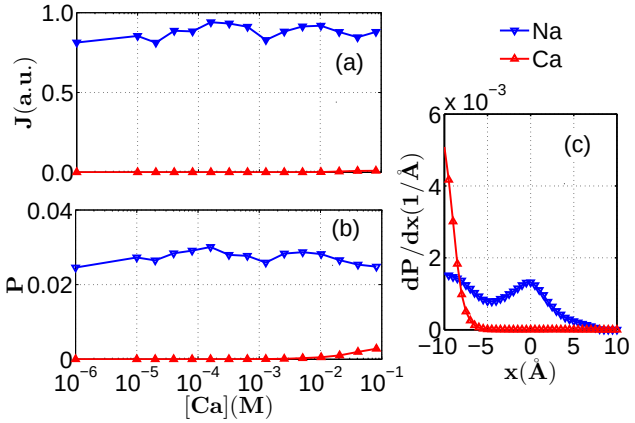

FIG. 3: (Color online) Band L0. Conduction and occupancy in a mixed salt bath with Na^+ (blue, point-down, triangles) and Ca^{2+} (red, point-up, triangles); the lines are guides to the eye. (a) Sodium and calcium currents J and (b) occupancies P (b) *vs.* the Ca^{2+} concentration $[Ca]$ for $[Na] = 30$ mM. L0 shows moderate sodium conductivity without the divalent block corresponding to AMFE. (c) Mutual occupancy profiles for Na^+ (blue peaked curve) and Ca^{2+} ions show that the Ca^{2+} ion cannot enter the channel.

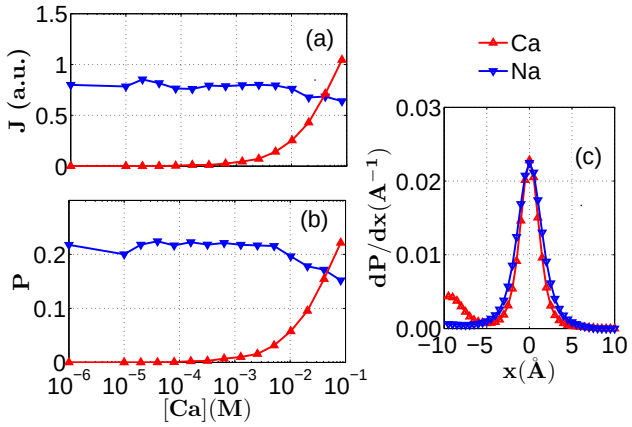

FIG. 4: (Color online) Band M0. Conduction and occupancy in a mixed salt bath with Na^+ (blue, point-down, triangles) and Ca^{2+}(red, point-up, triangles); the lines are guides to the eye. (a) Sodium and calcium currents J and (b) occupancies P *vs.* Ca^{2+} concentration $[Ca]$ in the non-selective M0 channel for $[Na] = 30$mM. M0 shows non-selective currents both in pure and mixed baths. (c) Mutual occupancy profiles for Na^+ and Ca^{2+} ions show an absence of blockade of Na^+ ions by the Ca^{2+} ions, and a time-shared occupancy mode.

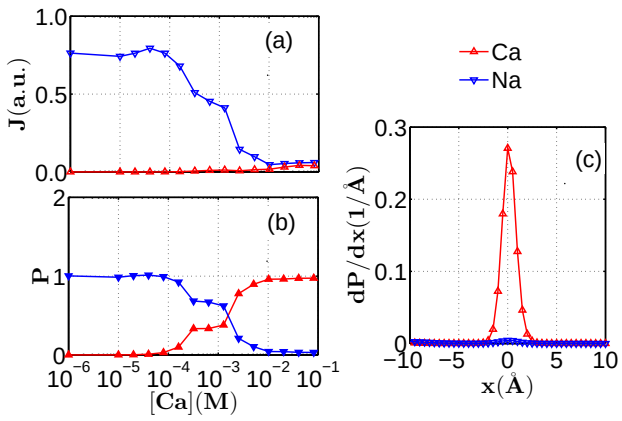

FIG. 5: (Color online) Band L1. Conduction and occupancy in a mixed salt bath with Na^+ (blue, point-down, triangles) and Ca^{2+} (red, point-up, triangles); the lines are guides to the eye. (a) Sodium and calcium currents J and (b) occupancies P *vs.* Ca^{2+} concentration $[Ca]$ in the sodium-selective L1 channel for $[Na] = 30$ mM. L1 shows strong blockade without AMFE at $P_{Ca} = 1$ with a threshold of $[Ca]_{50} \approx 1$ mM. (c) Mutual occupancy profiles for Na^+ and Ca^{2+} ions show substitution and blockade of Na^+ ions by the first Ca^{2+} ion which by itself completely occupies the channel.

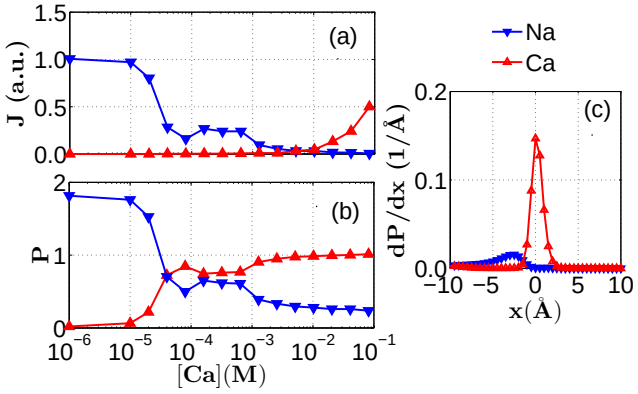

FIG. 6: (Color online) AMFE in a mixed salt bath for the M1 channel (reworked from [35]) with Na^+ (blue, point-down, triangles) and Ca^{2+} (red, point-up, triangles); the lines are guides to the eye. (a) Sodium and calcium currents J and (b) occupancies P *vs.* the Ca^{2+} concentration $[Ca]$ for $[Na] = 30$ mM. M1 shows strong blockade and AMFE at $P_{Ca} = 1$, with a threshold of $[Ca]_{50} \approx 30\mu$M. (c) Mutual occupancy profiles for Na^+ and Ca^{2+} show blockade of Na^+ ions by the first Ca^{2+} ion.

responds to barrier-less conductivity for Ca^{2+} (see Sec. III E).

The double-occupied sodium band L1 ($Q_f \approx 1.5 - 2.0e$) (Fig. 5) demonstrates high conductivity for pure sodium, zero conductivity for pure calcium and blockade of sodium current by calcium (a). As shown in (a),(b), the L1 band demonstrates a strong blockade of the sodium current J_{Na} by calcium ions with a blockade onset at $[Ca]_{50} \approx 1m$M. The blockade occurs after the first Ca^{2+} ion has occupied the selectivity filter: $P_{Ca} \to 1$ (plot (b)). Mutual occupancy profiles for Na^+ and Ca^{2+} show full substitution of Na^+ ions by the first Ca^{2+} ion (plot(c)). It is a sodium-selective channel with divalent block. This kind of selectivity corresponds to the wild type mammalian DEKA sodium channel [1, 12].

The narrow calcium selectivity peaks M1 ($Q_f \approx 3e$) and M2 ($Q_f \approx 5e$) (Fig. 2(c)) exhibit highly non-selective conductivity in a pure bath, and strong divalent block, followed by AMFE. This kind of selectivity is a trademark of calcium channels [2] identified with wild-type L-type and RyR calcium channels, respectively [35].

Fig. 6 presents the dependences of J and P on $[Ca]$ for the M1 band in a mixed salt configuration. As presented in (a),(b), M1 shows a strong blockade of the current J_{Na} of Na^+ ions with its onset at $[Ca]_{50} \approx 30\mu$M. The blockade occurs after the first Ca^{2+} ion has occupied the selectivity filter: $P_{Ca} \to 1$ as shown in (b). The mutual occupancy profiles for Na^+ and Ca^{2+} shown in (c) also indicate blockade of Na^+ ions by the first Ca^{2+} ion (plot(c)). This is a calcium-selective channel with single-ion calcium block. Strong blockade with a relatively low onset agrees qualitatively with the observed properties of the L-type channel [2]. The value of Q_f, and the conduction mechanism for M1, also correspond to the model [34] of the L-type channel (EEEE locus). Fig. 7 presents the dependences of J and P on $[Ca]$ for the M2 band in a mixed salt configuration. As shown in (a),(b), the M2 band with Q_f=5e shows a strong blockade of the current J_{Na} of Na^+ ions with its onset at $[Ca]_{50} \approx 150\mu$M. The blockade occurs after two Ca^{2+} ions have occupied the selectivity filter: $P_{Ca} \to 2$. This is a calcium-selective channel with double-ion calcium block. Divalent blockade with a relatively high onset and strong calcium current agrees qualitatively with the observed properties of the RyR calcium channel [4] or with the TPRV6 channel [5].

We thus arrive at the full identification scheme presented in Table I; it represents a completed version of the partial table in [35].

Within the framework of our scheme, an increase of negative fixed charge at the selectivity filter leads to an increase of calcium selectivity with the strict sequence: L0 (sodium selective, non-blocking channel) → M0 (non-selective cation channel) → L1 (sodium selective channel with divalent block) → M1 (calcium selective channel with divalent, blockade, AMFE). And *vice versa*, a decrease in the negative charge should change the selectivity from an L-type calcium channel to sodium, and from sodium to non-selective. The sodium L1 channel holds an intermediate position in the mutation scheme between the non-selective M0 channel and the calcium-selective M1 channel. This inference corresponds very well with the results of [12] where the DEKA sodium channel mutants chain was investigated for increasing Q_f. A similar increase of selectivity with increasing Q_f was obtained in [8, 15] but without the sharp selectivity peak at M1.

Comparison between the L1 and M1 conductivity-selectivity behavior shows a close similarity of their blockade mechanisms, but a significant difference between their calcium conductivities. Unlike the calcium-selective band M1, which exhibits narrow selectivity peaks, the sodium-selective band shows conduction/selectivity properties over a relatively wide range

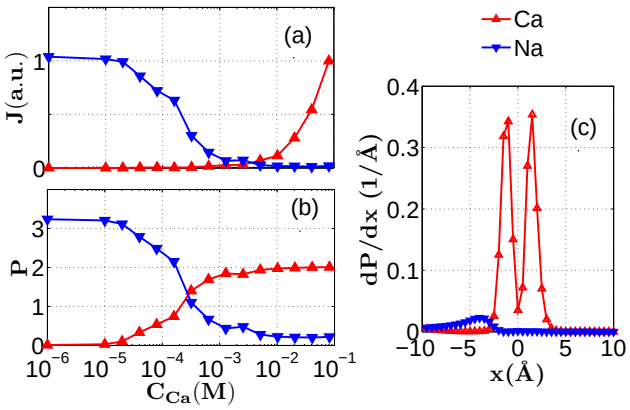

FIG. 7: ((Color online) AMFE in a mixed salt bath for the M2 channel (reworked from [35]) with Na^+ (blue, point-down, triangles) and Ca^{2+} (red, point-up, triangles); the lines are guides to the eye. (a) Sodium and calcium currents J and (b) occupancies P *vs.* the Ca^{2+} concentration $[Ca]_{50}$ for $[Na] =$ 30 mM. M1 shows strong blockade and AMFE at $P_{Ca} = 1$ with a threshold of $[Ca]_{50} \approx 150\mu$M. (c) Mutual occupancy profiles for Na^+ and Ca^{2+} ions show blockade of Na^+ ions by a pair of Ca^{2+} ions.

of Q_f around L1. This difference can be explained as being the result of barrier-less Ca^{2+} conductivity appearing in the narrow M1 band (see Sec. III D). In some sense, a sodium channel can be described as a sub-optimal calcium channel: the Ca^{2+} ion blocks the Na^+ current, but the Ca^{2+}-Ca^{2+} knock-on mechanism does not work.

C. Mutation-induced transitions between selectivity bands

The fact that we can identify simulated bands with different selectivity filter loci allows us to estimate putatively the *effective charges* represented by negatively charged glutamate (E) and aspartate (D) residues as $Q_E \approx 0.75e$ and $Q_D \approx 1.25e$, positively charged lysine (K) as $Q_K \approx 0.5e$ and neutral lanine (A) as $Q_A = 0$. These values differ from the nominal values measured or assigned for Q_X under physiological conditions [52]. The discrepancies may be connected in part to different (and unknown) ionisation states in particular ion channels [53, 54] with different localisation of the residues [52].

The identification of the bands allows us to establish a "charge scale" for different channels and different mutations (Table II). It is generally similar to [8, 15], though with different numbers for some residues and channels, particularly for the DEKA sodium channel assigned in [8, 15] as having $Q_f = 1e$. It allows us to describe/predict the known/possible results of mutations leading to substitutions of residues at the selectivity filter with residues with different charge, or to the elimination of particular residues. Note that our scale locates the DEKA sodium

TABLE I: Identification of conduction and selectivity bands of the model with known ion channels.

Conduction bands	**≈Fixed charge *(e)***	**Pure salt bath**		**Mixed salt bath**		**Channels**	**Locus / nominal charge**
		Na^+ current	Ca^{2+} current	Blockade	AMFE		
L0	0.5-0.75	Moderate	Low	No	No	Bacterial NaChBac [9] (?)	LESWAS(1e)
M0	1	Moderate	Moderate	No	No	Non-selective cation [50]; OmpF [15]	
L1	1.5-2	Low	High	Yes, by one Ca^{2+}	No	Nav sodium [1, 12], NLCN sodium channel [51]	DEKA(1e), EEKE(2e)
M1	3	High	High	Yes, by one Ca^{2+}	Yes	L-type calcium [3], NLCN calcium [51]	EEEE(4e)
M2	5	High	High	Yes, by two Ca^{2+}	Yes	RyR [4], TPRV6 [5]	DDDD(4e)

TABLE II: Mutation-induced selectivity transitions in calcium and sodium ion channels.

Channel transformation	**Locus changes/nominal charges**	**Band transition/charges**
Nav sodium → calcium selective [11]	DEKA (1e) → DEEA(3e)	L1(1.5e) → M1(3e)
Cav calcium → sodium-like mutant [3]	EEEE (4e) → DEDA (3e)	M1 (3e)→ L1 (1.5e)
NLCN calcium ↔ NLCN sodium [51]	EEEE (4e)↔ EEKE (2e)	M1(3e)↔ L1(1.5e)
Nonselective OmpF porin → calcium selective mutant [15]	RRRDE (2e)→ EEEE (4e)	M0(1e)→ M1(3e)
NaChBac sodium → nonselective → calcium selective [9]	LESWAS (1e)→ LEDWAS(2e)→ LDDWAD (3e)	L0 (0.6e) → M0(1e?) → M1(3e)

channel significantly closer to the EEEE L-type calcium channel, a position which corresponds to the results of mutant studies [11, 12].

The bacterial sodium NaChBac channel contains six amino acids in the pore domain (LESWAS) that participate in the selectivity filter. Replacing the amino acid residues adjacent to glutamic acid (E) by a negatively charged aspartate (D; LEDWAS) converted the Na^+-selective NaChBac to a Ca^{2+} and Na^+-permeant channel. When additional aspartates were incorporated (LDDWAD), the mutant channel exhibited voltage-gated Ca^{2+}-selective conductance [9]. Following our putative identification of NaChBac with the L0 band, the intermediate non-selective mutants can be connected to the M0 non-selective band and the resultant calcium-selective channel to the M1 band (see Table II).

The recently investigated NALCN channel is a member of the family of ion channels with four homologous repeat domains that include voltage-gated calcium and sodium channels. NALCN appears in two variants with selectivity filter residues that resemble either calcium channels (EEEE) or sodium channels (EKEE or EEKE), controlled by a single gene. [51]. We can tentatively identify the EEKE channel with the L1 band and EEEE with the M1 band. Reversible transformations between these states can be identified as L1↔M1 transitions.

Table II lists some known mutation transformations together with their attributions within the framework of our model.

An appropriate point mutation of the DEKA sodium channel ($Q_f \approx 1e$) converts it into a calcium-selective channel with a DEEA locus [11]. Our scheme identified this result with the L1 ($Q_f = 1.5e$)→M1 ($Q_f = 3e$) transition.

The essentially non-selective bacterial OmpF porin with its RRRDE locus can be converted into a Ca^{2+}-selective channel by the introduction of two additional glutamates in the constriction zone; the resultant mutant contains a DEEE-locus and exhibits an Na^+ current with a strongly increased sensitivity to 1 mM Ca^{2+} [15]. We can identify this transformation with the M0 ($Q_f = 1.0e$)→M1 ($Q_f = 3e$) transition.

Thus our identification scheme provides straightforward explanations for the outcomes of several mutant studies. Some results still seem to lie outside the scope of our model, however, e.g. the change of the ions' permeation/selectivity by a simple permutation of the residues at the selectivity filter, or the intermediate results of [9].

The calcium-selective M1 band exhibits a narrow resonance-like selectivity peak. We can conclude that any single mutation of the calcium channel which influences Q_f should destroy its specific calcium selectivity. It corresponds well with the facts that EEEE signature for the L-type channel is highly conserved [2] and that mu-

tations in the genes responsible for the selectivity filter motif lead to numerous diseases [13].

The resonance-like nature of calcium selectivity is particularly interesting in connection with the recently discovered NavAb sodium channel which possesses the same EEEE locus as the calcium L-type channel but exhibits sodium-selective permeation behavior [7, 10]. In the context of our model, this paradox could be explained in terms of the geometry difference (relatively small length of selectivity filter, or large radius), and possibly different protonation, of the residues at the selectivity filter [52–54]. In relation to the geometry difference, we should bear in mind that the bands disappear when L decreases to 8 Å or R reaches to 4.5 Å [35], so that calcium selectivity could drastically decrease. Another plausible explanation relates to possible variations in protonation of residues for different channels and therefore to slightly different effective charge for nominally the same loci [2, 34]. Due to the narrowness of the calcium-selective band even small changes of total charge could convert it to sodium channel. Clarification of these questions will require further experimental research and more detailed simulations.

D. Energetics of single-ion conduction and selectivity bands L0 and M0

We now investigate the energetics of calcium and sodium conductivity in our model, and show explicitly that a barrier-less permeation mechanism underlies the appearance of the conduction and selectivity bands.

Fig. 8 shows that barrier-less conductivity for cations of particular valence (the calcium M0 band is drawn) appears as the result of a balance between the self-repulsion of the dielectric boundary force and the electrostatically amplified attraction to the negative fixed charge. The self-repulsion is proportional to Q_i^2, whereas the attraction is proportional to $Q_i \times Q_f$. Thus a variation of Q_f can significantly change the resultant profile. This kind of barrier-less selectivity was suggested earlier for the Gramicidin channel [20, 27, 55].

Fig. 8(a) illustrates the fact that, for small $Q_f <$ M0, self-repulsion dominates and the channel is not permeable by any ion; and that, for large Q_f ($Q_f >$ M0), attraction dominates and the ionic dynamics is then controlled by Kramers escape with an exponential dependence on ΔE. Between these two extremes an optimal point Q_{opt} ($Q_{opt} = 0.87e$ for Ca^{2+} ions) exists where $\Delta E = |E_{max} - E_{min}|$ is minimized with the appearance of a barrier-less ($\Delta E \sim k_B T$) profile for the moving ion. Sodium ions exhibit a similar pattern but with $Q_{opt} = 0.45e$ providing for valence selectivity between monovalent Na^+ and divalent Ca^{2+} ions (see Fig. 9).

Fig. 8(b) shows that for $Q_f = M0$ the self-potential barrier of the dielectric boundary force is balanced by electrostatic attraction to the fixed charge Q_f, resulting in a low barrier with $\Delta E \sim k_B T$.

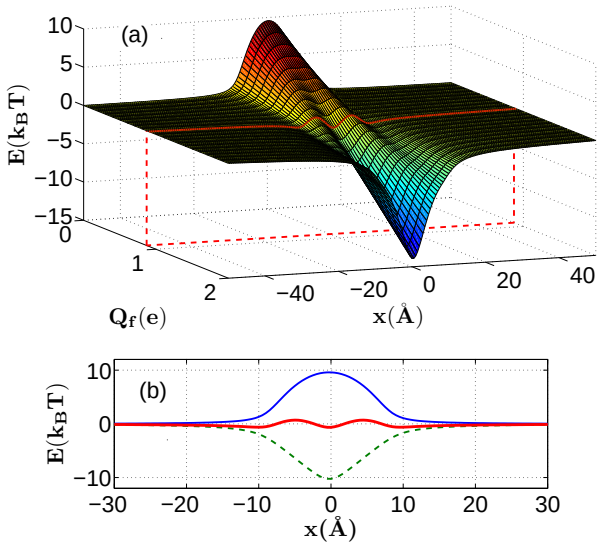

FIG. 8: (Color online) The appearance of a barrier-less path for the channel M0. (a) The electrostatic potential energy profile along the channel's $x-$axis is plotted *vs.* the fixed charge Q_f. The energy differences across the profile are minimal at a particular value of $Q_f = Q_{opt}$. (b)This optimal profile for permeation (red) appears as the result of a balance between repulsion by the dielectric boundary force (blue) and attraction to the fixed charge (green, dashed).

To compare the results of electrostatic calculations and BD simulations we introduce simplified kinetic model allowing us to connect energy difference along energy profile with current J and occupancy P.

for single-occupied channel and assuming the absence of back-flow we get linear dependence for J vs P in Kramers rate approximation : $J = k_0 \cdot P$ where k_0 stands for escape rate. Coulomb interaction between ion inside channel and ions in the bath and at the mouth makes k0 being dependent on concentration [25, 56] and so leads to deviations of J from linear dependence on P.

We assume generalized Kramers equation for k_0 in the vicinity of M0 or L0: $k_0 \approx D/L^2 exp(-\Delta E/k_B T)$ and get the resulting expression for current J:

$$J = k_0 P \approx D/L^2 exp(-\Delta E/k_B T) \cdot P \qquad (3)$$

or assuming that P=const

$$J = J_0 * exp(-\Delta E/k_B T) \qquad (4)$$

where J_0 is reference current.

We will use (4) to compare J vs Q_f dependencies obtained from electrostatics and BD simulations.

Fig. 9 compares the energetics and BD results for singly-occupied sodium L0 and calcium M0 bands. The electrostatically calculated dependences of ΔE on Q_f reveal sharp minima at $Q_{opt} = 0.45e$ for the L0 (plot (a))

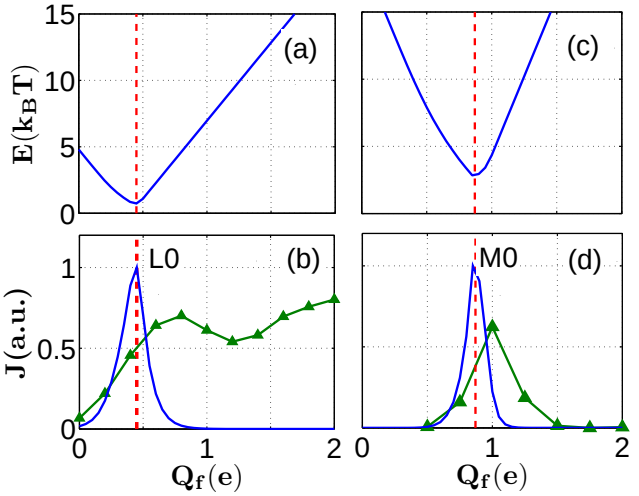

FIG. 9: (Color online) Energetics and Brownian dynamics of the singly-occupied sodium L0 and calcium M0 bands. (a) The L0 band potential energy *vs.* the fixed charge Q_f. The energy difference along the profile shows a clear minimum at $Q_{opt} = 0.45e$. (b) The peak in the sodium current J *vs.* Q_f calculated from electrostatics (blue curve) lies relatively close to the BD-simulated L0 peak (green point-up triangles, detrended). (c) The M0 potential energy *vs.* the fixed charge Q_f. The energy difference along the profile show a sharp minimum at $Q_{opt} = 0.87e$. (d) The peak in the calcium current J *vs.* Q_f calculated from electrostatics (blue curve) lies close to the BD-simulated M0 peak. (green point-down triangles).

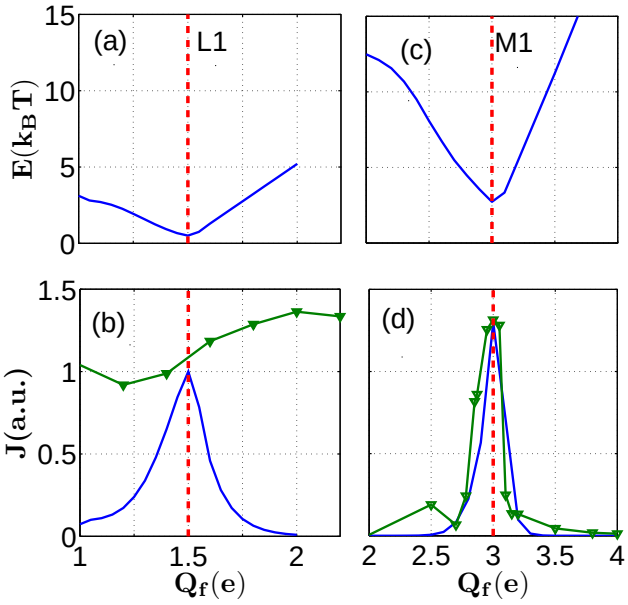

FIG. 10: (Color online) Energetics and Brownian dynamics of the double-ion sodium L1 and calcium M1 bands. (a) The L1 band potential energy *vs.* the fixed charge Q_f. The energy difference along the profile shows a wide minimum at $Q_{opt} = 1.5e$. (b) The peak in the sodium current J *vs.* Q_f calculated from electrostatics is shifted down compared to the very weak BD-simulated conductance peak L1 (green point-down triangles). (c) The M1 band potential energy *vs.* fixed charge Q_f. The energy difference along the profile show a deep minimum at $Q_{opt} = 3e$. (d) The peak in the calcium current J *vs.* Q_f calculated from electrostatics (blue curve) lies close to the BD-simulated M0 peak in selectivity (green point-down triangles).

and at $Q_{opt} = 0.9e$ for the M0 (plot c)) bands. The calcium band M0 exhibits a sharper Q_f dependence because of having a twice-larger charge.

Fig. 9(b),(d) compare the shapes and positions of electrostatically calculated conductivity peaks ($J \sim J_0 \exp(\Delta E/k_B T)$) with those obtained from the BD simulations. The positions of these peaks are in reasonable agreement, although the BD simulated peaks are shifted towards higher Q_f, probably due to kinetic effects related to (3) and changing of P and k_0. These results support our inference that the resonance-like L0 and M0 bands maxima are attributable to barrier-less conduction. The conduction maximum for L0 shown in (b) is broadened towards higher Q_f due to its overlap with L1 and to the slower exponent in J for sodium. It leads to non-selective conduction for M0, as discussed above.

E. Energetics of double-ion barrier-less conduction bands L1 and M1

The double-ion sodium selectivity band L1 is identified with the DEKA sodium channel. The double-ion calcium band M1 is identified with the L-type calcium channel [34, 35].

Multi-ion conductance appears when the selectivity filter potential well becomes too deep (about $60k_B$T for Ca^{2+} in the vicinity of M1) making the channel impermeable when occupied by just one ion. Instead, conduction events occur via a double-ion knock-on conduction mechanism. This mechanism is caused by the electrostatic interaction between simultaneously captured ions, a process that is particularly effective for divalent Ca^{2+} ions [21, 34].

The interacting calcium or sodium ions move simultaneously, in a coordinated manner, enabling escape to occur over a potential barriers of minimal height on the 2D potential energy surface (PES) [57, 58]. The PES approach allows one to describe double-ion conduction as the potential motion of a quasi-particle along an optimal stochastic trajectory on a PES [30, 38, 59], thereby reducing the problem of double-ion conduction to the case already discussed, i.e. the 1D movement of a particle (in this case a "super-ion") in an electrostatic field.

We exploit this approach to show explicitly that the resonance-like conduction and selectivity of the M1 calcium channel and the L1 sodium channel occur through a barrier-less, multi-ion, conduction mechanism. To study valence selectivity we construct both homogeneous Ca^{2+}-

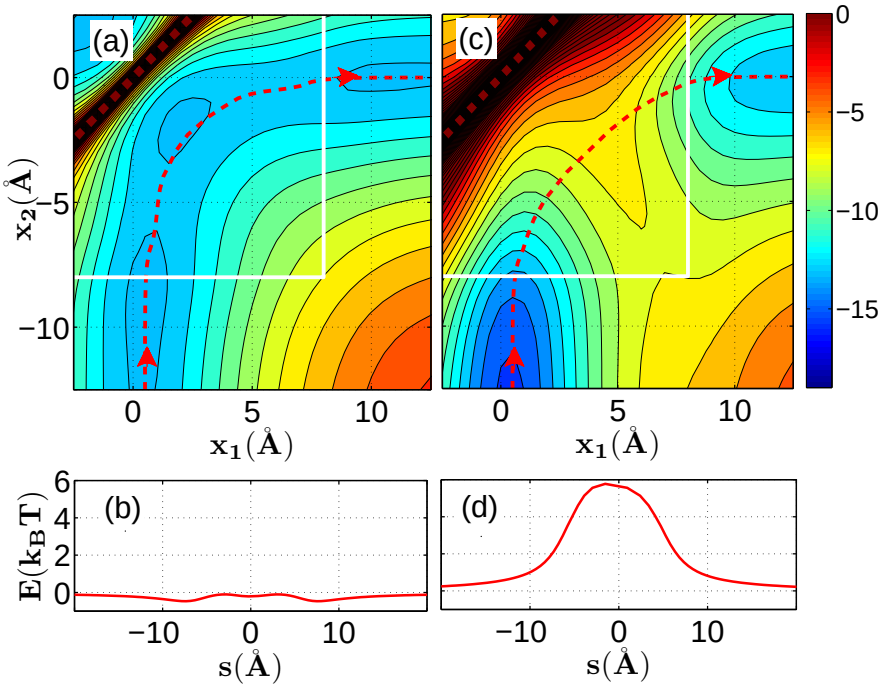

FIG. 11: (Color online) (a) Double-ion Na^+-Na^+ potential energy surface (PES) for the model channel with $Q_f = M1(1.5e)$, shown as a contour plot. The contour separation is $1k_BT$, and the colorbar labels are in units of k_BT. The diagonal ridge in the upper-left corner represents the electrostatic barrier along the main diagonal of the map $x_1 = x_2$. The map area related to the selectivity filter is limited by the white lines. The optimal trajectory S (red dashed line) traverses two orthogonal valleys in the direction shown by the arrows and represents a "knock-on" event. The first ion initially captured at the center of the selectivity filter is pushed and substituted for by the second ion arriving at the channel mouth. (b) The potential energy E profile along S demonstrates almost barrier-less permeation. Plots (c),(d) show the same quantities for the heterogeneous Ca^{2+}-Na^+ double-ion: the binding site is initially occupied by a Ca^{2+} ion that should be pushed by a Na^+ ion. The optimal trajectory S navigates via two valleys separated by a saddle which creates an intermediate potential barrier ($\Delta E \approx 6k_BT$), corresponding to divalent blockade of Na.

Ca, Na^+-Na, and heterogeneous Na^+-Ca^{2+} double-ion PESs, find the optimal (minimal energy change) stochastic paths, and calculate the energy profiles along these paths.

Fig. 10(a) shows the calculated dependence of ΔE on Q_f for the L1 band (DEKA sodium channel), revealing a smooth minimum at $Q_{opt} = 1.5e$. These data are obtained from the analysis of optimal trajectories for the electrostatic PES. A comparison of the current calculated from Kramers' approximation with that obtained from the BD simulations is shown in (d). The BD simulated maximum in the sodium current at $Q_{opt} = 2e$ is very weak and shifted up relative to the point of barrier-less conductance as shown in (b). The discrepancy can be attributed to kinetics effects and to the obviously strong overlap between the different sodium bands (see Fig. 2).

Fig. 10(c) shows the calculated dependence of ΔE on Q_f for the M1 band (L-type calcium channel), revealing a sharp minimum at $Q_{opt} = 3e$. These data are obtained from an analysis of optimal trajectories for the electrostatic PES. A comparison between the current calculated from the Kramers approximation, with that obtained from the BD simulations is shown in (d). The good agreement between the peaks confirms that the maximum of selectivity in the double-occupied M1 band corresponds to the point of barrier-less conductivity.

Fig. 11 presents Na^+-Na^+ and Ca^{2+}-Na^+ PES maps, optimal trajectories, and corresponding energy profiles, for Q_f=L1, at the point of barrier-less conductivity. Plots (a),(b) show the Na^+-Na^+ PES map and energy optimal trajectory S corresponding to a knock-on event, navigating two orthogonal valleys from South to East on the PES. The energy profile along S is almost flat (the energy difference along the optimal path does not exceed $1k_BT$) corresponding to fast, barrier-less, permeation.

In contrast, the heterogeneous Ca^{2+}-Na^+ PES for L1 (Fig. 12(c),(d)) exhibits a high potential barrier ($\Delta E \approx 6k_BT$) for a sodium ion trying to knock-on a calcium ion, which needs to be overcome by thermal activation. This is the PES-language explanation for calcium blockade in the DEKA sodium channel.

The pattern for Ca^{2+}-Ca^{2+} permeation is rather similar but all effects are much more pronounced. Fig. 12 presents Ca^{2+}-Ca^{2+} and Ca^{2+}-Na^+ PES maps, optimal trajectories and corresponding energy profiles for Q_f=M1, at the point of maximum Ca/Na^+ selectivity.

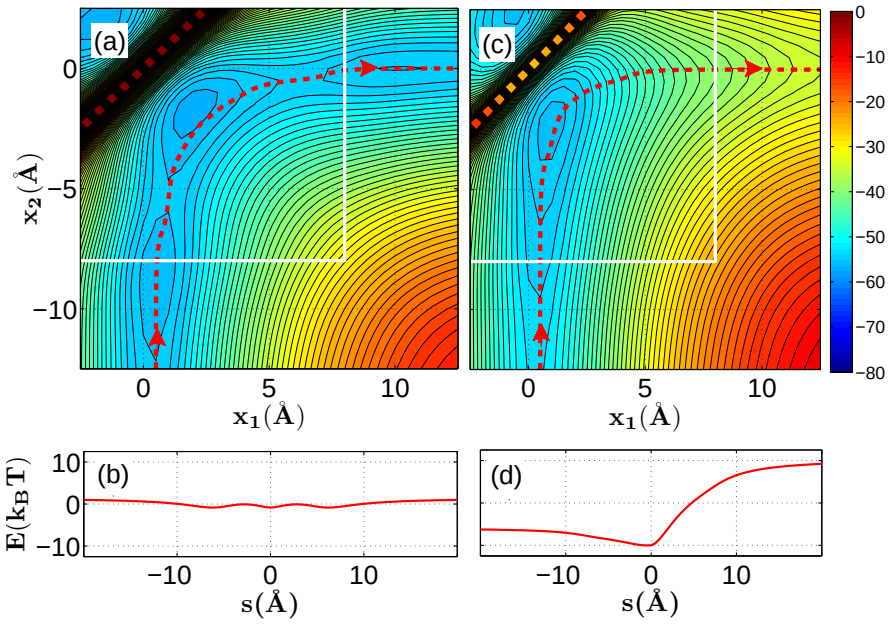

FIG. 12: (Color online) (a) Double-ion Ca^{2+}-Ca^{2+} potential energy surface (PES) for the model channel with $Q_f = M1(3.0e)$, shown as a contour plot. The contour separation is $1k_BT$, and the colorbar labels are in units of k_BT. The diagonal ridge in the left upper corner represents the electrostatic barrier along the main diagonal of the map $x_1 = x_2$. The map area related to the selectivity filter is limited by the white lines. The optimal trajectory S (red dashed line) traverses two deep ($\approx 60k_BT$) orthogonal valleys in the direction shown by the arrows, and represents a "knock-on" event. The first ion initially captured at the center of the selectivity filter is pushed out and substituted for by the second ion arriving at the channel mouth. (b) The potential energy E profile along S demonstrates almost barrier-less permeation ($\Delta E < 2kBT$). Plots (c),(d) show the same quantities for the heterogeneous Ca^{2+}-Na^{+} double-ion: the binding site is initially occupied by a Ca^{2+} ion that should be pushed by a Na^{+} ion. The optimal trajectory S navigates via deep valley ended by high potential barrier ($\Delta E \approx 20kBT$), corresponding to deep divalent blockade of Na^{+} current.

Fig. 12 (a),(b) shows the Ca^{2+}-Ca^{2+} PES map and the energy-optimal trajectory S, navigating two deep orthogonal valleys. The energy profile along S is almost flat (the energy difference along the optimal path does not exceed 1-2 k_BT) corresponding to fast barrier-less permeation.

Again, in contrast, the heterogeneous Ca^{2+}-Na^{+} PES for M1 (Fig. 12(c),(d)) exhibits a impermeable high potential barrier $\Delta E \approx 20k_BT$ for a sodium ion trying to knock-on calcium ion. This barrier needs to be overcome by thermal activation. This is the PES-language explanation for calcium blockade and AMFE in the EEEE calcium channel.

These results confirm that the resonance-like calcium band M1 corresponds to barrier-less, double-ion, conduction for Ca^{2+} ions and a deep blockade of Na^{+} ions, thereby resolving the selectivity *vs.* conductivity paradox.

In terms of our simple model, there is of course no essential difference between a biological ion channel and an artificial nanopore of similar geometry (radius R and length L) and surface charge Q_f. Such nanopores may be expected to demonstrate similar conductivity and selectivity features and a number of practical applications can be envisaged.

IV. CONCLUSIONS

In summary, Brownian dynamics simulations of ionic conductance for a generic model of the calcium-sodium channel family for different values of the negative charge at the selectivity filter $Q_f = 0 - 6.5e$ have revealed a strictly ordered sequence of selectivity bands of increased calcium selectivity: L0=0.5-0.7e (sodium selective, non-blocking channel) $\rightarrow$ M0=1e (non-selective cation channel) $\rightarrow$ L1=1.5-2e (sodium selective, blocking channel) $\rightarrow$ M1=3e (calcium selective, blocking channel with AMFE, single-ion block) $\rightarrow$ M2=5e (calcium selective, blocking channel with AMFE, double-ion block).

Our preliminary identification of bands presented in [35] has been confirmed, and completed as follows: L0 corresponds to the NavChBac bacterial sodium channel; M0 to the non-selective cation channel or to OmpF porin; L1 to the eukaryotic DEKA sodium channel; M1 to the L-type EEEE calcium channel; and M2 to the RyR DDDD calcium channel.

The completed identification scheme accounts for the experimentally observed mutation transformations of conductivity/selectivity between the non-selective channel, sodium channels and calcium channels. It is suggested that mutation-induced transformations appear as

transitions between different rows in the identification table. The scheme provides a unified and straightforward explanation for the results of several mutation studies in the Ca^{2+}/Na^{+} family of ion channels and in OmpF porin.

Our investigations of the energetics of conduction and valence selectivity show explicitly, by consideration of optimal trajectories on potential energy surfaces, that the multi-ion conduction bands of the calcium/sodium channels arise as the result of single- and multi-ion barrier-less conduction. These resonance-like effects are much more pronounced for the divalent calcium bands M0 and M1.

Our results confirm the crucial influence of electrostatic interactions on the conduction and Ca^{2+}/Na^{+} valence selectivity of calcium and sodium ion channels, thereby resolving the celebrated selectivity *vs.* conductivity paradox. They have also demonstrated the surprisingly broad applicability of generic ion channel models. We speculate that they they may readily be extended to describe the permeation and selectivity properties of artificial nanopores.

Acknowledgements

The research was supported by the Engineering and Physical Sciences Research Council UK (grant No. EP/G070660/1).

[1] B. Hille, *Ionic Channel Of Excitable Membranes* (Sinauer Associates, Sunderland, MA, 2001), 3rd ed.
[2] W. A. Sather and E. W. McCleskey, Ann. Rev. Physiol. **65**, 133 (2003).
[3] J. Yang, P. T. Ellinor, W. A. Sather, J. F. Zhang, and R. W. Tsien, Nature **366**, 158 (1993).
[4] D. Gillespie, Biophys. J. **94**, 1169 (2008).
[5] G. Owsianik, K. Talavera, T. Voets, and B. Nilius, Annu. Rev. Physiol. **68**, 685 (2006).
[6] T. Vora, B. Corry, and S. H. Chung, Biochim. Biophys. Acta Biomem. **1668**, 106 (2005).
[7] J. Payandeh, T. Scheuer, N. Zheng, and W. A. Catterall, Nature **475**, 353 (2011).
[8] E. Csányi, D. Boda, D. Gillespie, and T. Kristf, Biochim. Biophys. Acta (BBA) – Biomembranes **1818**, 592 (2012).
[9] L. X. Yue, B. Navarro, D. J. Ren, A. Ramos, and D. E. Clapham, J. Gen. Physiol. **120**, 845 (2002).
[10] J. Payandeh, T. M. G. El-Din, T. Scheuer, N. Zheng, and W. A. Catterall, Nature **486**, 135 (2012).
[11] S. H. Heinemann, H. Teriau, W. Stuhmer, K. Imoto, and S. Numa, Nature **356**, 441 (1992).
[12] T. Schlief, R. Schonherr, K. Imoto, and S. H. Heinemann, Eur. Biophys. J. & Biophys. Lett **25**, 75 (1996).
[13] D. L. Burgess and J. L. Noebels, in *Molecular and Functional Diversity of Ion Channels and Receptors*, edited by B. Rudy and P. Seeburg (1999), vol. 868 of *Ann. N.Y. Acad. Sci.*, pp. 199–212.
[14] S. E. Koch, I. Bodi, A. Schwartz, and G. Varadi, J. Biol. Chem. **275**, 34493 (2000).
[15] H. Miedema, A. Meter-Arkema, J. Wierenga, J. Tang, B. Eisenberg, W. Nonner, H. Hektor, D. Gillespie, and W. Meijberg, Biophys. J. **87**, 3137 (2004).
[16] D. Boda, W. Nonner, M. Valisko, D. Henderson, B. Eisenberg, and D. Gillespie, Biophys. J. **93**, 1960 (2007).
[17] D. Boda, W. Nonner, D. Henderson, B. Eisenberg, and D. Gillespie, Biophys. J. **94**, 3486 (2008).
[18] C. A. Hübner and T. J. Jentsch, Human Mol. Genet. **11**, 2435 (2002).
[19] A. L. Hodgkin and R. D. Keynes, J. Physiol. **128**, 61 (1955).
[20] B. Roux, T. Allen, S. Berneche, and W. Im, Quart. Rev. Biophys. **37**, 15 (2004).
[21] P. Hess and R. W. Tsien, Nature **309**, 453 (1984).
[22] C. M. Armstrong and J. Neytonc, Ann. New York. Acad. Sci. **635**, 18 (1991).
[23] S. O. Yesylevskyy and V. N. Kharkyanen, Chem. Phys. **312**, 127 (2005).
[24] D. G. Luchinsky, R. Tindjong, I. Kaufman, P. V. E. McClintock, and R. S. Eisenberg, J. Stat. Mech. **P01010** (2009).
[25] R. Tindjong, I. Kaufman, P. V. E. McClintock, D. G. Luchinsky, and R. S. Eisenberg, Fluct. Noise Lett. **11**, 1240016 (2012).
[26] W. Nonner, L. Catacuzzeno, and B. Eisenberg, Biophys. J. **79**, 1976 (2000).
[27] B. Nadler, U. Hollerbach, and R. S. Eisenberg, Phys. Rev. E **68**, 021905 (2003).
[28] B. Corry, T. Vora, and S. H. Chung, Biochimica Et Biophysica Acta-Biomembranes **1711**, 72 (2005).
[29] J. Zhang, A. Kamenev, and B. I. Shklovskii, Phys. Rev. Lett. **95**, 148101 (2005).
[30] V. N. Kharkyanen, S. O. Yesylevskyy, and N. M. Berezetskaya, Phys. Rev. E **82**, 051103 (2010).
[31] B. Eisenberg, Physiol. **28**, 28 (2013).
[32] B. Eisenberg, in *Adv. Chem. Phys.*, edited by S. A. Rice and A. R. Dinner (Wiley-Blackwell, Malden, MA, 2012), vol. 148 of *Advances in Chemical Physics*, pp. 77–223.
[33] R. S. Eisenberg, Biophys J. **104**, 000 (2013).
[34] B. Corry, T. W. Allen, S. Kuyucak, and S. H. Chung, Biophys. J. **80**, 195 (2001).
[35] I. Kaufman, D. G. Luchinsky, R. Tindjong, P. V. E. McClintock, and R. S. Eisenberg, Phys. Biol. **10**, 026007 (2013).
[36] R. S. Eisenberg, I. Kaufman, D. G. Luchinsky, R. Tindjong, and P. V. E. McClintock, Biophys J. **104**, 358a (2013).
[37] R. S. Eisenberg, in *New Developments in Theoretical Studies of Proteins*, edited by R. Elber (World Scientific, Singapore, 1996), pp. 269–357.
[38] M. I. Dykman, P. V. E. McClintock, V. N. Smelyanskiy, N. D. Stein, and N. G. Stocks, Phys. Rev. Let. **68**, 2718 (1992).
[39] J. Giri, J. E. Fonseca, D. Boda, D. Henderson, and B. Eisenberg, Phys. Biol. **8**, 026004 (2011).
[40] B. Corry, Energy & Env. Sci. **4**, 751 (2011).

[41] B. Corry, S. Kuyucak, and S.-H. Chung, J. Gen. Physiol **114**, 597 (1999).
[42] L. A. Richards, A. I. Schäfer, B. S. Richards, and B. Corry, Small **8**, 1701 (2012).
[43] B. Nadler, T. Naeh, and Z. Schuss, SIAM J. Appl. Math. **62**, 433 (2001).
[44] D. G. Luchinsky, R. Tindjong, I. Kaufman, P. V. E. McClintock, and R. S. Eisenberg, in *Electrostatics 2007*, edited by Green, N. (2009), vol. 142 of *J. Phys. Conf. Series*.
[45] D. P. Tieleman, P. C. Biggin, G. R. Smith, and M. S. P. Sansom, Quart. Rev. Biophys. **34**, 473 (2001).
[46] K. Nelissen, V. R. Misko, and F. M. Peeters, EPL (Europhys. Lett) **80**, 56004 (2007).
[47] R. Garcia-Fandiño and M. S. P. Sansom, Proc. Natl. Acad. Sci. USA **109**, 6939 (2012).
[48] H. Miedema, in *Biomimetic Membranes for Sensor and Separation Applications*, edited by C. H''elix-Nielsen (Springer, Dordrecht, 2012), pp. 63–86.
[49] B. Corry, PeerJ **16**, DOI10.7717/peerj.16 (2013).
[50] R. Guinamard, M. Paulais, S. Lourdel, and J. Teulon, BBA–Biomembranes **1818**, 1135 (2012).
[51] A. Senatore, A. Monteil, J. van Minnen, A. B. Smit, and J. D. Spafford, PLoS ONE **8** (2013).
[52] J. J. Finnerty, R. Eisenberg, and P. Carloni, J. Chem. Theor. Comput. **9**, 766 (2013).
[53] G. D. Cymes, Y. Ni, and C. Grosman, Nature **438**, 975 (2005).
[54] S. Varma and E. Jakobsson, Biophys. J. **86**, 690 (2004).
[55] D. G. Levitt, Biophys. J. **22**, 209 (1978).
[56] B. Nadler, Z. Schuss, U. Hollerbach, and R. S. Eisenberg, Phys. Rev. E. **70**, 051912 (2004).
[57] P. S. R. Ganesh, B. Chanda, S. K. Gupta, M. K. Mathew, and J. Chandrasekhar, Prot. Struct. Funct. Genet. **38**, 384 (2000).
[58] D. Gordon and S.-H. Chung, J. Phys. Chem. B **116**, 14285 (2012).
[59] R. Elber, D. P. Chen, D. Rojewska, and R. Eisenberg, Biophys. J. **68**, 906 (1995).
[60] The protein residues are amino acids, of which aspartate (D) and glutamate (D) have negatively charged side chains. Others that we mention here are lysine (K), which has a positively charged side chain, as well as alanine (A), leucine (L), tryptophan (W) and serine (S).
[61] Note that, strictly, it is low-barrier conduction: the potential barriers are still present albeit greatly reduced in size, as discussed in Sec. III. For convenience, however, we will follow the convention of referring to "barrier-less conduction."